# High-pressure and high-temperature studies on oxide garnets

Hong Hua, Sergey Mirov, and Yogesh K. Vohra
*Department of Physics, University of Alabama at Birmingham (UAB), Birmingham, Alabama 35294-1170*
(Received 26 February 1996; revised manuscript received 7 May 1996)

We report high-pressure and high-temperature studies on a series of oxide garnets of chemical composition $A_3B_2C_3O_{12}$. The members of this family investigated are gadolinium scandium gallium garnet (GSGG), gadolinium gallium garnet (GGG), and yttrium aluminum garnet (YAG). The GSGG and GGG are doped with both neodymium and chromium while the YAG is doped only with neodymium. Photoluminescence, synchrotron x-ray-diffraction, and laser heating studies were carried out in a diamond-anvil cell. Variety of optical sensors (ruby, Sm-doped YAG) and x-ray pressure marker (copper) were employed for pressure measurement. Pressure-induced amorphization was observed in GSGG at $58\pm3$ GPa and GGG at $84\pm4$ GPa by x-ray-diffraction studies. The photoluminescence studies show only gradual broadening of emission bands through the amorphization transition. On increasing pressure beyond amorphization, very broad and featureless emission bands were observed in the fluorescence spectra at $77\pm2$ GPa for GSGG and at $88\pm2$ GPa for GGG. Laser heating of the pressure-induced amorphous phase in GSGG caused recrystallization to the stable cubic phase. High-pressure x-ray study on YAG shows that it retains cubic phase up to $101\pm4$ GPa. A pressure-volume relation for each member of the oxide garnet at ambient temperatures is presented, structural transformation mechanisms, and application of oxide garnets as pressure sensors are also discussed.
[S0163-1829(96)08833-9]

## I. INTRODUCTION

Oxide garnets belong to the family of solid-state laser materials. High-pressure optical studies and crystallographic studies on garnets are expected to yield interesting data on the phase stability of the cubic structure and dopants' energy levels. Some doped oxide garnet materials have been applied as optical pressure sensors.[1,2] Our recent result of GSGG under high pressure using the synchrotron x-ray-diffraction technique documented the amorphization of gadolinium scandium gallium garnet (GSGG) at $58\pm3$ GPa.[3] This phenomena motivated us to investigate other garnet materials' properties under high pressure. Using synchrotron x-ray diffraction, microphotoluminescence, and laser heating techniques, we conducted high-pressure investigations on a family of oxide garnets. In this paper, we will present structural data, fluorescence data, and recrystallization studies on several oxide garnets.

The three materials studied in this paper, $Gd_3Sc_2Ga_3O_{12}$ (GSGG), $Gd_3Ga_5O_{12}$ (GGG), and $Y_3Al_5O_{12}$ (YAG), all belong to oxide garnets of formula $A_3B_2C_3O_{12}$, where $A$ denotes the dodecahedral, $B$ the octahedral, and $C$ the tetrahedral sites.[2,4] Oxide garnets can achieve systematic changes in the crystal-field strength by variation of the unit-cell size. Along the series YAG ($Y_3Al_5O_{12}$), YGG ($Y_3Ga_5O_{12}$), GGG ($Gd_3Ga_5O_{12}$), GSAG ($Gd_3Sc_2Al_3O_{12}$), GSGG ($Gd_3Sc_2Ga_3O_{12}$), LLGG ($La_3Lu_2Ga_3O_{12}$) the unit cell's size increases and the crystal-field strength decreases progressively.[4] GSGG is a derivative of GGG, in which gallium that is octahedrally coordinated is replaced with scandium.

As shown above, we can change the crystal-field strength of the garnets via changing the chemical composition. But this method can only give a set of discrete points along the crystal-field strength continuum and potential complications can arise from chemical inequivalence.[5] Now, with the high-pressure technique, we are able to tune the crystal-field strength encountered by the dopant ion continuously, thus avoid the complicating effects due to the different chemical compositions.[2,5] In addition, the current development of laser heating techniques,[6] when combined with the high-pressure technique, enables us to investigate the transformations in materials at the condition of the earth's interior.

In this paper, we will review our past and recent works on GSGG, i.e., synchrotron x-ray-diffraction and microphotoluminescence high-pressure experiments on crystalline GSGG and also the laser heating experiment on the amorphous GSGG sample that was quenched from high pressure. Besides that, we will report our results on synchrotron x-ray-diffraction and microphotoluminescence high-pressure studies of GGG and YAG, which were carried out at ambient temperature.

## II. THEORETICAL

In this section, we will give some theoretical introduction to (1) pressure-induced amorphization and (2) pressure effects on dopant's energy-level splitting.

### A. Amorphization

In 1984, Mishima, Calvert, and Whalley[7] discovered the amorphization of $H_2O$ ice I at 1 GPa and 77 K. Since then, this crystalline-to-amorphous ($c\rightarrow a$) transformation in the solid state has been the focus of intense study and has been documented in more materials[7,8] using x-ray-diffraction and spectroscopic methods.

Various models have been proposed so far to understand the thermodynamics and driving mechanism for this $c\rightarrow a$ transition. It has been suggested[8] that this transition is a con-

 

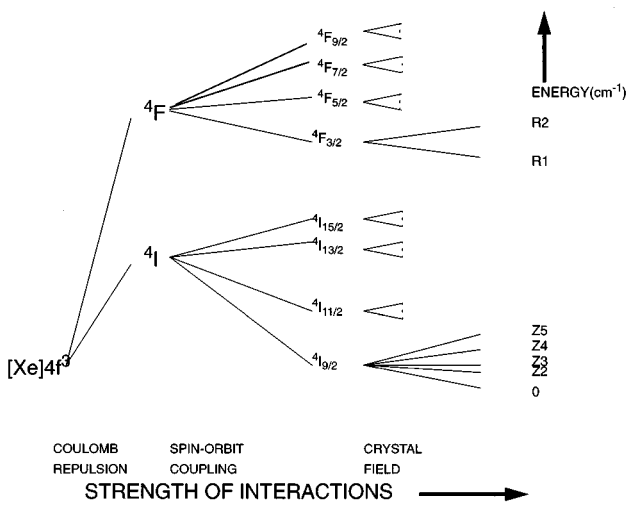


FIG. 1. Schematic representation of the energy levels of $Nd^{3+}$ in garnet showing the effects of Coulomb repulsion, spin-orbit coupling, and crystal-field interaction.

sequence of a competition between the close packing and long range order: the application of high pressure promotes close packing but the shape of the basic block in the crystal may not favor this, thus further compression may result in steric hindrances and ultimately destabilizing the parent crystal structure. Also, for the substances which can amorphize under pressure, there exists a three-level free-energy diagram, with kinetic barriers (Fig. 1 in Ref. 8). In this diagram, a crystalline solid is first driven to a high-energy state, then the free energy of this crystalline state can be lowered by forming either a metastable amorphous state or a more energetically favored crystalline state. However, the existence of the kinetic barrier between metastable and stable phases will promote formation of metastable phase at room temperature. The amorphization of garnet can be documented directly in x-ray-diffraction studies, where the sharp diffraction peaks due to crystalline phase broaden abruptly during the amorphization.

### B. Dopant's energy-level splitting

For doped garnet, the observed photoluminescence spectrum is composed of the emission bands of the dopants. Pressure effect on the dopant's emission in a crystalline environment such as garnet is determined by different contributions, like electronic shielding, hybridization of wave functions, strength, and symmetry of the crystal field.[9] Figure 1 is a schematic example of the energy-level splitting of the dopant $Nd^{3+}$ in garnet host. There are three major contributions to the observed fine structures in the dopant energy levels: Coulomb repulsion, spin-orbit coupling, and the crystal-field effects. The pressure-dependent variation of the balance between these interactions yields three shifts such as (1) the shift of the $LS$ manifolds with respect to each other due to variations in the Coulomb interaction (2) the shift of the centers of each crystal-field-split $J$ manifold for a given $LS$ value which results from the variations of the spin-orbit coupling and (3) the shift of the Stark levels (of one LSJ manifold) with respect to each other due to the variation of the crystal field in strength and symmetry. In a first point-charge approximation, the energy separations between the Stark levels of one $|L,S,J\rangle$ increase as the crystal-field strength increases. The deviation of Stark splitting from this tendency is attributed to phase or site symmetry change, second-order effect, etc.

The dopant, rare-earth ion, $Nd^{3+}$ $(4f^3)$ in garnet lattice is generally assumed to be located in the $D_2$ site symmetry (which belongs to orthorhombic symmetry) and all Stark levels of it can be represented by the same symmetry label $^2\Gamma_5$.[4] For state $^4F_{3/2}$, cubic symmetry gives no splitting, while symmetry lower than cubic will give the splitting to $R_1$ and $R_2$. The ground state $^4I_{9/2}$ split into five levels: $Z_1$ (which is always set to 0), $Z_2$, $Z_3$, $Z_4$, and $Z_5$. Corresponding to different crystalline environment the dopant is in, the energy values will be slightly different and it is reflected in the photoluminescence spectra as measured by us in Fig. 2(a). The bands in Fig. 2(a) are indexed according to the notation of the energy levels defined in Fig. 2(b). Table I summarizes the data for energy-level splittings of states $^4F_{3/2}$, $^4I_{9/2}$ of $Nd^{3+}$ in GSGG, GGG, and YAG.

For dopant-transition-metal ion $Cr^{3+}$ $(3d^3)$, the lowest excited state can be either $^2E$ or $^4T_2$, depending on the strength of the octahedral crystal field it is in.[2,10] The lowest excited state is $^2E$ in a strong crystal field and $^4T_2$ in a weak crystal field. The ground state is $^4A_2$. Since the transition $^2E \rightarrow {}^4A_2$ is spin forbidden, $^4T_2 \rightarrow {}^4A_2$ is spin allowed, $^2E$ gives rise to the sharp $R$-line emission, while $^4T_2$ gives rise to broad emission bands. For the intermediate crystal-field strength systems, $^4T_2$ and $^2E$ levels are close to each other in energy. In this paper, for GSGG and GGG, which are $Cr^{3+}$ doped, a broad $^4T_2$ emission bands is observed at ambient conditions.

## III. EXPERIMENTAL

### A. Sample preparation

GSGG, GGG single crystals (both containing approximately 0.6 at. wt. % for $Nd^{3+}$ and 1.0 at. wt. % for $Cr^{3+}$) and YAG single crystals (doped with approximately 1.0 at. wt. % of $Nd^{3+}$) were grown at the General Physics Institute of Russian Academy of Sciences. GSGG is green, GGG is slightly green, and YAG is almost transparent in appearance.

We employed diamond-anvil cell (DAC) to generate static high pressure. DAC is now the most powerful ultrahigh-pressure device which can generate the static pressure up to 400 GPa. The sample is placed between the flat parallel faces of two opposed diamond anvils and is subjected to pressure when a force is applied on the anvils. The gasket between two parallel diamond flat planes can hold the sample and provide a uniform pressure distribution and support. Three different DAC's were used in the present series of experiments. The first cell ($DAC_1$) is with diamonds of 300 $\mu$m culet. Spring steel gaskets with the 75 $\mu$m sample hole were prepared for holding the sample. The second cell ($DAC_2$) is with diamonds of 600 $\mu$m culet and the sample hole in the spring steel gasket was 150 $\mu$m. In the third cell ($DAC_3$), the two diamonds are of different size. The top diamond is of 80 $\mu$m central flat with 7° bevel and 350 $\mu$m culet, while the bottom one is of 300 $\mu$m culet, and the sample hole was 50 $\mu$m. In the rest of this report, we will use the notations $DAC_1$, $DAC_2$, $DAC_3$ to specify these three

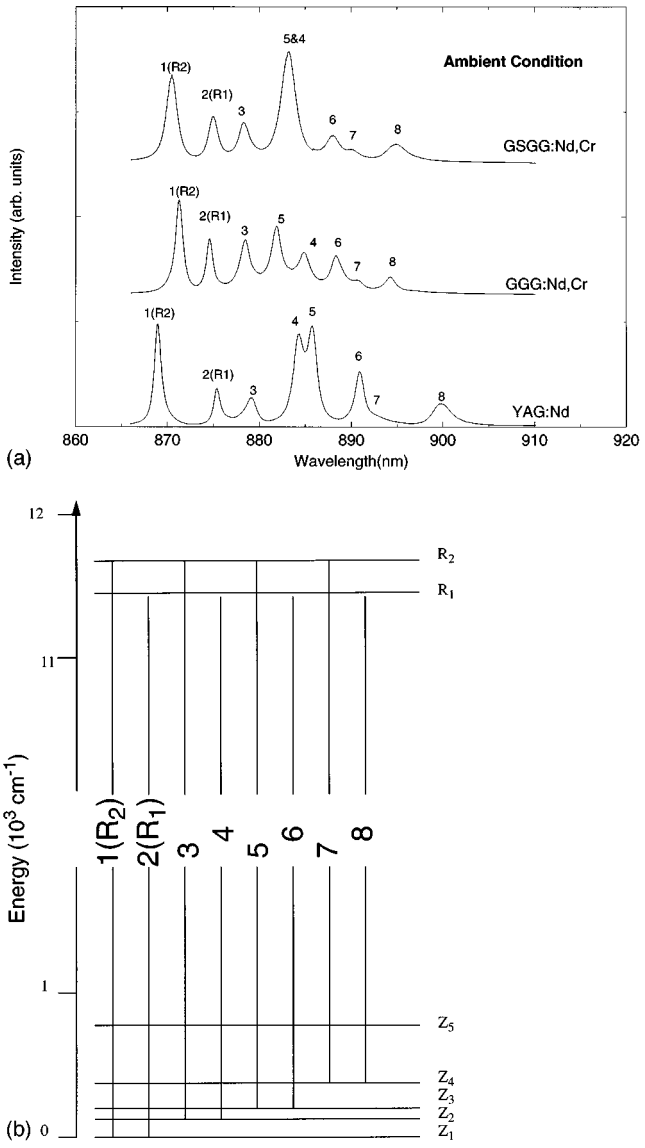


FIG. 2. (a) A comparison of $Nd^{3+}$ emission corresponding to $^4F_{3/2} \rightarrow {}^4I_{9/2}$ transition in different garnet lattice hosts: GSGG, GGG, and YAG. (b) Various transitions in the $^4F_{3/2}$ and $^4I_{9/2}$ manifolds for $Nd^{3+}$ in garnet lattice hosts.

DAC's, respectively. Pressure sensor (or standard) chips of small size 3–5 $\mu$m were placed inside the hole together with the sample, both were surrounded by pressure medium. In optical experiments, ruby[11] on Sm:YAG (Ref. 1) was used as pressure sensor, while in x-ray experiments, copper was employed as pressure standard.[12,13] In all experiments, a 4:1 methanol-ethanol mixture served as pressure medium that provided the hydrostatic pressures below 15 GPa.

### B. Photoluminescence

Photoluminescence data were recorded during both compression and decompression of all the samples investigated. The 514.5 or 457.9 nm wavelength of an argon-ion laser was utilized to excite the photoluminescence spectra. A micro-Raman and photoluminescence spectrometer as described in Ref. 14 was used in all these experiments. This spectrometer consists of two adjacent spectrometers, one 0.6 m long with a 1200 grooves/mm grating, and the other 0.2 m long with 150 grooves/mm and 600 grooves/mm gratings. With the 1200 grooves/mm grating, the spectral resolution is $\sim 3$ cm$^{-1}$ (in the unit of wave number), and $\sim 1.5$ nm (in the unit of wavelength) for the 150 grooves/mm grating. The laser beam was focused to a spot size of 5–10 $\mu$m on the samples in DAC.

Various experiments described in this paper are summarized in Table II. For photoluminescence experiments on GSGG, three slightly different experiments were performed. The first one (Exp. I) was carried in $DAC_1$ and employed ruby as pressure sensor. The excitation source was 514.5 nm argon laser line. Since in this experiment, the ruby's $R$ lines were so strong that they masked the GSGG's $R$ lines, in the second experiment (Exp. II) we substitute the ruby crystal by a Sm:YAG crystal and used the 457.9 nm laser to achieve better excitation. For the third experiment (Exp. III), we used $DAC_2$ and used ruby crystal as pressure sensor, the excitation source was 514.5 nm laser line. The highest pressures for these three experiments were $77\pm2$, $68\pm1$, and $51.0\pm0.5$ GPa, respectively.

For photoluminescence of GGG with high pressure, two experiments were conducted. In one experiment (Exp. IV), we employed $DAC_3$ and used the 514.5 nm laser to achieve excitation. In another experiment (Exp. V), we used $DAC_1$ and the 457.9 nm laser line. Ruby was employed as pressure sensor in both experiments. The highest pressure for these two experiments are $94\pm4$ GPa and $86\pm2$ GPa, respectively. YAG photoluminescence study (Exp. VI) was done with $DAC_1$ and the pressure was calibrated against ruby $R$ lines. The 514.5 nm argon laser line was the excitation source. The highest pressure we reached was $72\pm1$ GPa.

### C. X-ray diffraction

The energy-dispersive x-ray-diffraction studies were carried out at either the X-17C beam line, National Synchrotron Light Source (NSLS), Brookhaven National Laboratory or at the B1 station, Cornell High Energy Synchrotron Source (CHESS) in Cornell University. Copper was employed as an internal pressure standard[12,13] in all the x-ray-diffraction experiments. We label these experiments performing on GSGG, GGG, and YAG as Exp. VII, Exp. VIII, and Exp. IX,

TABLE I. Experimental data for the observed $R$ and $Z$ lines for the $Nd^{3+}$: $^4F_{3/2}$ and $^4I_{9/2}$ in the photoluminescence spectra of GSGG, GGG, and YAG. Energy units are in wave numbers (cm$^{-1}$).

| | YAG | GGG | GSGG |
|---|---|---|---|
| $^4F_{3/2}$ ($R$ lines) | 11 423, 11 507 | 11 442, 11 485 | 11 424, 11 492 |
| $^4I_{9/2}$ ($Z$ lines) | 0, 132, 200, 311, 852 | 0, 93, 178, 253, 772 | 0, 105, 167, 263 |

TABLE II. The summary of various high-pressure experiments conducted on oxide garnets. The diamond geometry, laser excitation source, pressure calibrant, and the highest pressure attained in various experiments are included.

| Experiment | Sample | DAC | Excitation source | Pressure calibrant | Highest pressure (GPa) | Note |
|---|---|---|---|---|---|---|
| Exp. I | GSGG:Nd,Cr | $DAC_1$ | $Ar^+$514.5 nm | Ruby $R_1$ line | 77 ±2 | Loss of fine structure |
| Exp. II | GSGG:Nd,Cr | $DAC_1$ | $Ar^+$457.9 nm | Sm YAG Y lines | 68 ±1 | Loss of fine structure |
| Exp. III | GSGG:Nd,Cr | $DAC_2$ | $Ar^+$514.5 nm | Ruby $R_1$ line | 51.0±0.5 | |
| Exp. IV | GGG:Nd,Cr | $DAC_3$ | $Ar^+$514.5 nm | Ruby $R_1$ line | 94 ±4 | Loss of fine structure |
| Exp. V | GGG:Nd,Cr | $DAC_1$ | $Ar^+$457.9 nm | Ruby $R_1$ line | 86 ±2 | |
| Exp. VI | YAG:Nd | $DAC_1$ | $Ar^+$514.5 nm | Ruby $R_1$ line | 72 ±1 | |
| Exp. VII | GSGG:Nd,Cr | $DAC_1$ | X ray | Copper | 65 ±1 | Amorphization |
| Exp. VIII | GGG:Nd,Cr | $DAC_2$ | X ray | Copper | 84 ±4 | Amorphization |
| Exp. IX | YAG:Nd | $DAC_2$ | X ray | Copper | 101 ±4 | |
| Exp. X | GSGG:Nd,Cr | $DAC_1$ | Nd:YAG laser | | | Following Exp. I |

respectively. The highest pressures we have obtained are 65±1 GPa in Exp. VII, 84±4 GPa in Exp. VIII, and 101±4 GPa in Exp. IX.

### D. Laser heating

A laser heating facility is added to the micro-Raman/Photoluminescence Spectrometer described above. The laser heating source is a Quantronix Model 116EBW-0/CW-20 Nd:YAG laser operating at 1.06 $\mu$m with cw power of 20 W. The sensitive CCD detector in the spectrometer can cover 400 nm to 1.1 $\mu$m spectrum range. This laser heating system can heat the sample under high pressure in the DAC up to 3000–4000 K. Typical sample area to be heated is approximately 50 $\mu$m in diameter. A laser heating experiment (Exp X) was conducted after Exp. I, when the sample was totally quenched from the highest 77±2 GPa. The $Q$-switched Nd:YAG laser beam was used to heat the sample. Blackbody emission spectrum was taken during the laser heating, while photoluminescence spectrum of the sample was taken with a 514.5 nm line of an argon-ion laser after the heating.

### E. Pressure and temperature calibration

In photoluminescence experiments, the pressure was calibrated against either ruby $R$ lines or Sm:YAG Y lines. For two of our samples, $Nd^{3+}$,$Cr^{3+}$:GSGG and $Nd^{3+}$,$Cr^{3+}$:GGG a problem arises when we use ruby as the pressure calibrant because ruby's $R$ lines and associated broadband emissions are mixed with the emission of $Cr^{3+}$ ions in GSGG and GGG samples in the range of 690–720 nm. Since ruby $R$-line emission is very strong, great care was taken to separate the ruby $R$ lines from the $R$ emission of the sample by performing high-resolution (using 1200 grooves/mm grating) scans in the $R$-line region. The pressure error is estimated from the full width at half maximum of the ruby $R_1$ line, which affects the accuracy of $R_1$ position reading.

In x-ray experiments, pressure calibration was carried out using copper's modified universal equation of state[12,13] (MUEOS) as described below:

$$\ln H = \ln B_0 + \eta(1-X) + \beta(1-X)^2, \tag{1}$$

where $X^3 = V/V_0$ is the volume compression, $\eta = 1.5(B_0' - 1)$, and $H = PX^2/[3(1-X)]$. $V_0$, $B_0$, and $B_0'$ are the atomic volume, isothermal bulk modulus, and the first pressure derivative of the bulk modulus at ambient pressure, respectively. The MUEOS with parameters $B_0 = 143.7$ GPa, $B_0' = 3.904$, and $\beta = 13.77$ was fitted to the shock-wave data of copper up to 240 GPa.[12,13] The pressure error is related to the maximum fitting error of the copper diffraction peak location.

For laser heating experiment, we followed the procedure developed in Ref. 15 and measured the temperature by measuring the energy spectrum of the emitted light from the material.[15] From Wien's law, energy spectrum of the emitted light from the material with temperature $T$ is

$$I(\lambda,T) = F(\lambda)\varepsilon(\lambda,T)(2C_1/\lambda^5)\exp(-C_2/\lambda T), \tag{2}$$

where $F(\lambda)$ is the efficiency of the measurement system, $\varepsilon(\lambda,T)$ is the emissivity of the material, and $C_1, C_2$ are constants. By measuring the emission from a material with temperature $T_0$, we can determine $J(\lambda,T)$ and $\omega(\lambda)$ as follows:

$$J(\lambda,T) = \ln\{I(\lambda,T)\lambda^5/[2C_1F(\lambda)\varepsilon_0(\lambda,T_0)]\}, \tag{3}$$

$$\omega(\lambda) = C_2/\lambda. \tag{4}$$

We can get the following equation:

$$J(\lambda,T) = (-1/T)\omega(\lambda) + \ln[\varepsilon(\lambda,T)/\varepsilon_0(\lambda,T_0)]. \tag{5}$$

The emissivity, which is a function of wavelength and temperature does not change much within the visible spectral region. Thus from Eq. (5), if we assume the ratio $\varepsilon(\lambda,T)/\varepsilon_0(\lambda,T_0)$ is a constant independent of $\lambda$ within the observed range, the spectrum becomes a straight line when it is plotted as a function of $J$ vs $\omega$. The temperature $T$ can be calculated from the slope of the straight line. The temperature error was calculated from averaging over several scans under the same heating condition.

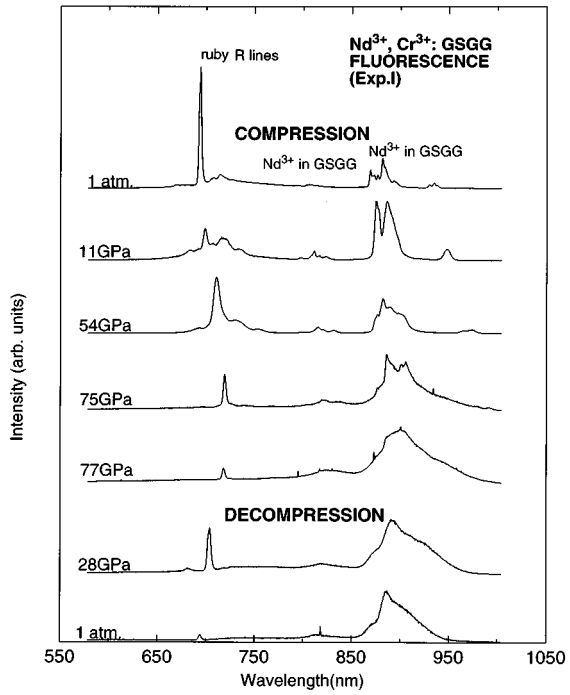


FIG. 3. Pressure dependence of the emission in $Nd^{3+}$, $Cr^{3+}$:GSGG at room temperature, excited by argon 514.5 nm laser, ruby is the pressure sensor (Exp. I). The spectrum covers the broad spectral range of 570–990 nm.

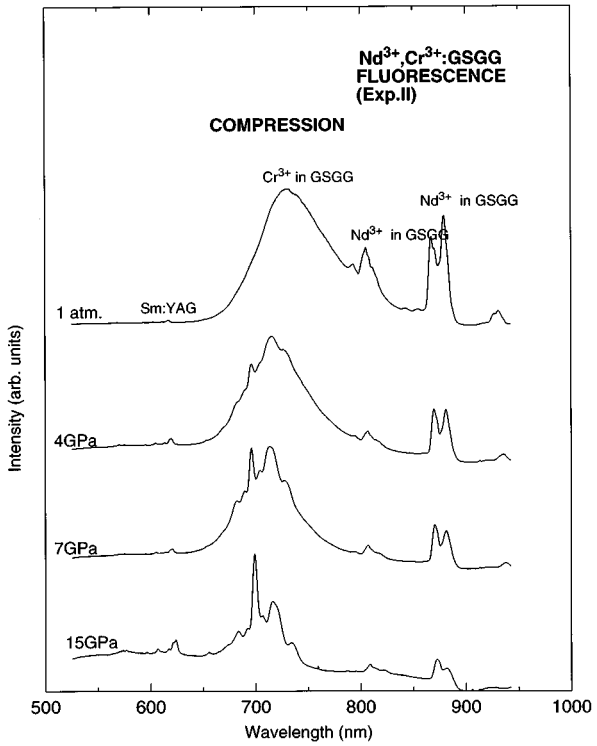


FIG. 4. Emission in $Nd^{3+}$, $Cr^{3+}$:GSGG at room temperature, excited by argon 457.9 nm, showing that emergence of $R$ lines of the sample under high pressure, Sm:YAG is the pressure sensor (Exp. II). The sharp features appear in $Cr^{3+}$ manifold on increasing pressure.

## IV. EXPERIMENTAL RESULTS

### A. GSGG

#### *1. Photoluminescence*

a. Broad spectral range. In all the optical experiments on GSGG Exp. I, II, and III using 150 grooves/mm to cover a broad spectral range from 570 to 990 nm, $Nd^{3+}$ emission bands were shown to broaden with increasing pressure, as presented in Fig. 3 with the typical spectra taken from Exp. I. Additional pressure effect on $Cr^{3+}$ transition-induced emission was obtained in Exp. II as represented in Fig. 4. It should be added that in the spectral range of 570–990 nm three distinct emissions from the sample are apparent in Figs. 3 and 4. A broadband in the range of 650–850 nm indicates the dominance of the $Cr^{3+}$ $^4T_2 \rightarrow {}^4A_2$ transition, while two sets of sharp bands in the range of 770–840 nm and 850–900 nm are due to $Nd^{3+}$ $^4F_{5/2}$ and $^2H_{9/2} \rightarrow {}^4I_{9/2}$, $^4F_{3/2} \rightarrow {}^4I_{9/2}$ transitions respectively. In Exp. I and Exp. III, where ruby was used as pressure sensor, the ruby $R$ lines lie in the left region of the broadband (Fig. 3), while in Exp. II, where Sm:YAG was the pressure sensor instead, the Sm:YAG Y lines lie in the region of 595–630 nm (Fig. 4). In Exp. II, sharp emission bands (which corresponds to $Cr^{3+}$ $^2E \rightarrow {}^4A_2$ transition) emerged at about 10 GPa and was seen superimposed on the broad $Cr^{3+}$ $^4T_2 \rightarrow {}^4A_2$ transition band (Fig. 4).

Upon compression, the emission bands show gradual broadening at the beginning. As pressure increased from $75\pm1$ to $77\pm2$ GPa in Exp. I (Fig. 3), and from $65\pm1$ to $68\pm2$ GPa in Exp. II (Fig. 4), all the narrow bands caused by $Cr^{3+}$ and $Nd^{3+}$ transitions in GSGG broadened significantly, leaving three featureless broad bands at the above three regions. Since the sample stayed transparent and no visible change has been observed in the sample absorbance throughout the experiment,[3] we attribute this broadening to the change of site symmetry or coordination for the dopants in GSGG, and the totally broadening of sharp emission bands to the loss of fine structure.

b. High-resolution study of the $Nd^{3+}$ $^4F_{3/2} \rightarrow {}^4I_{9/2}$ transition. The 1200 grooves/mm grating was used to study the high-pressure effect on $Nd^{3+}$ $^4F_{3/2} \rightarrow {}^4I_{9/2}$ emission bands (which dominates in the range of 860–920 nm) in detail in all the three experiments. Following the changes of those emission bands [$R_2$, $R_1$, 3, 4, 5, 6 as in Fig. 2(a)], we found that all bands broadened gradually as pressure increased. $R_2$ band became the strongest and sharpest one at $75\pm1$ GPa. As pressure increased from $75\pm1$ to $77\pm2$ GPa, all the sharp bands (including $R_2$ band) broadened significantly and merged together. The whole merged band was retained on decreasing pressure.

c. High-resolution study of $Cr^{3+}$ emission: from $^4T_2 \rightarrow {}^4A_2$ to $^2E \rightarrow {}^4A_2$ transition. In Exp. II, as pressure increased from ambient to $4.0\pm0.5$ GPa, in the spectral range of 650–850 nm, the broad emission band due to $Cr^{3+}$ $^4T_2 \rightarrow {}^4A_2$ transition, shift toward shorter wavelength (Fig. 4). As shown in Fig. 5, using 1200 grooves/mm grating to scan that spectral region, we can see clearly that below $4.0\pm0.5$ GPa, that is only a very broadband emission. However, narrow $^2E \rightarrow {}^4A_2$ emission bands emerge at $7.0\pm0.5$ GPa. At $16\pm1$ GPa, the underlying broadband emission is almost completely eliminated. After that, the sharp bands broaden and shift toward longer wavelength as pressure in-

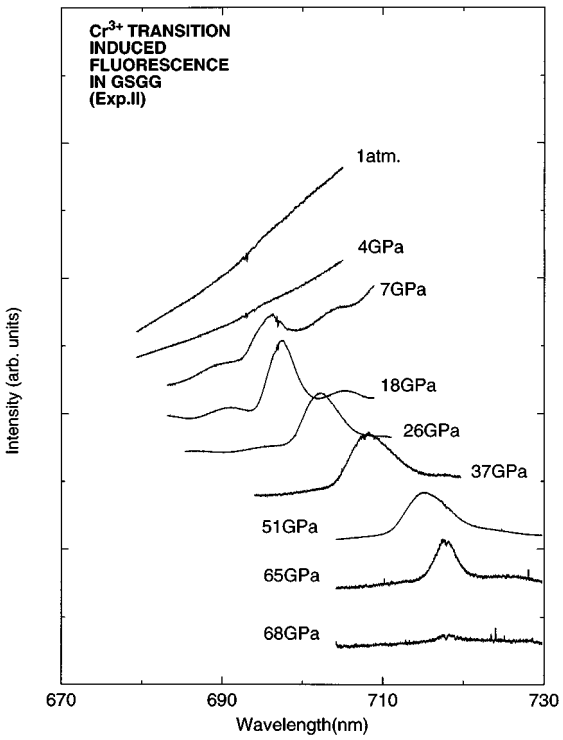


FIG. 5. High-resolution scans of the photoluminescence spectra of the $R$ lines of $Cr^{3+}$ in $Nd^{3+}$, $Cr^{3+}$:GSGG at high pressure (Exp. II).

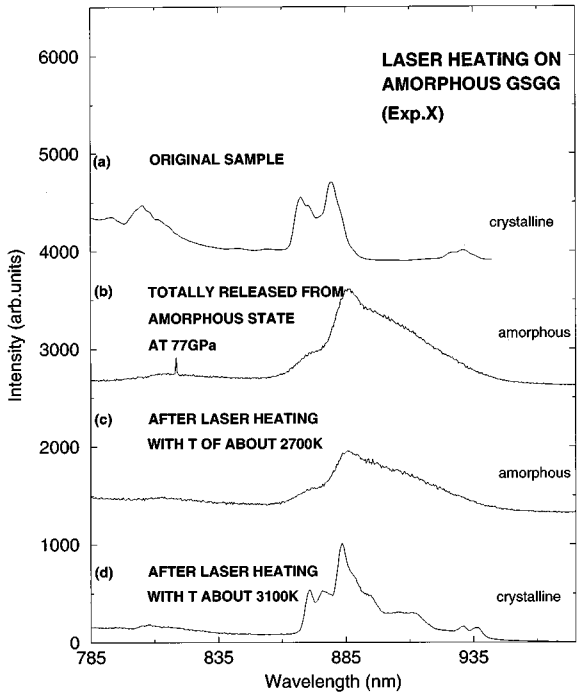


FIG. 6. Laser heating experiment on amorphous GSGG produced by Exp. I (a) original crystalline sample for comparison (b) retained amorphous sample at ambient condition after high-pressure experiment up to 77 GPa (c) amorphous state after laser heating with temperature of about 2700 K (d) recrystallization of sample after laser heating with temperature of about 3100 K.

creases. At pressure above 68±2 GPa, the narrow band becomes featureless and centers at about 718 nm. The $R$ lines of Nd,Cr:GSGG are not resolved in this experiment.

#### *2. X-ray diffraction*

The synchrotron x-ray-diffraction experiment clearly demonstrated that GSGG becomes amorphous at 58±3 GPa and the quenched sample remains amorphous, as previously discussed in Ref. 3. Also, during compression up to 55.5 ±0.5 GPa (which is before amorphization), the sample remains in cubic phase. The lattice parameter changes from 12.53±0.02 Å at ambient pressure to 11.84±0.04 Å at 55.5 ±0.5 GPa, with the compression of 16.0±0.5%.

#### *3. Laser heating*

Figure 6 demonstrates the recrystallization of amorphous GSGG using laser heating technique (Exp. X). Spectrum (a) in Fig. 6 represents the original crystalline material, while spectrum (b) in Fig. 6 represents the quenched amorphous sample from the high-pressure experiment (Exp. I). After heating the sample using Nd:YAG laser current of 26 A (the calibrated temperature is 2700±200 K), the sample retained its amorphous state [Fig. 6(c)]. When increasing the current to 28 A (the temperature we calibrated is about 3100±100 K), the sample transformed to a crystalline state [Fig. 6(d)]. Comparing spectra (a) and (d) in Fig. 6, the transformed sample is nearly identical to the original. This similarity is clearer in Fig. 7 using higher resolution (1200 grooves/mm grating) to scan the $Nd^{3+}$:$^4F_{3/2}\rightarrow{}^4I_{9/2}$ emission bands. Thus, we conclude that after the amorphous GSGG sample was heated to a temperature of 3100±100 K, it recrystallized to the original cubic phase.

### B. GGG

#### *1. Photoluminescence*

Similar emission band broadening phenomena occurred in a GGG sample as in the GSGG sample. Typical spectra taken from Exp. IV using 150 grooves/mm gratings are shown in Fig. 8. At ambient conditions, we observe two sets of sharp emission bands in the regions of 780–850 nm and 855–910 nm, due to $Nd^{3+}$:$^4F_{5/2}$, $^2H_{9/2}\rightarrow{}^4I_{9/2}$ and $Nd^{3+}$:$^4F_{3/2}\rightarrow{}^4I_{9/2}$ transitions in the sample, respectively. The broad $Cr^{3+}$:$^4T_2$, $^2E\rightarrow{}^4A_2$ emission bands of GGG in the region of 670–750 nm are masked by strong ruby $R$ lines. As pressure increases, the two sets of sharp bands gradually broaden and shift toward longer wavelength. But as the pressure increases from 86±2 to 90±3 GPa, the sharp bands significantly broaden and leave two featureless broad bands in the two regions of 800–850 nm and 850–1000 nm.

A higher resolution 1200 grooves/mm grating scan was used to investigate the $Nd^{3+}$ $^4F_{3/2}\rightarrow{}^4I_{9/2}$ transitions in the region of 860–910 nm in detail. In Exp. IV, it is found that the emission bands broaden and shift toward longer wavelength as pressure increases. At 65.5±1.0 GPa, all the bands expect for $R_2$ line become very broad. When pressure increased from 86±2 to 90±3 GPa, even the $R_2$ line broadened significantly, leaving a very broadband in the whole region. Since the sample remains transparent throughout the

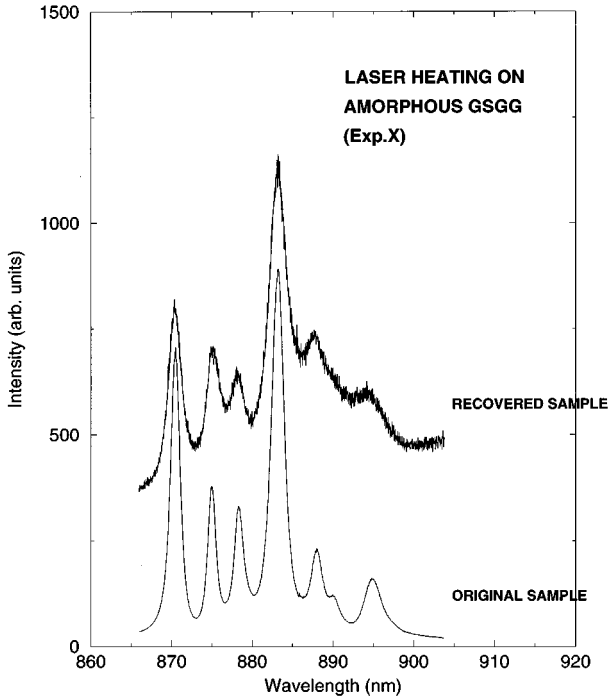


FIG. 7. High-resolution scans of the $Nd^{3+}$ $^4F_{3/2}\rightarrow{}^4I_{9/2}$ photoluminescence spectra for the original crystalline GSGG and laser heated sample (recrystallized from amorphous phase).

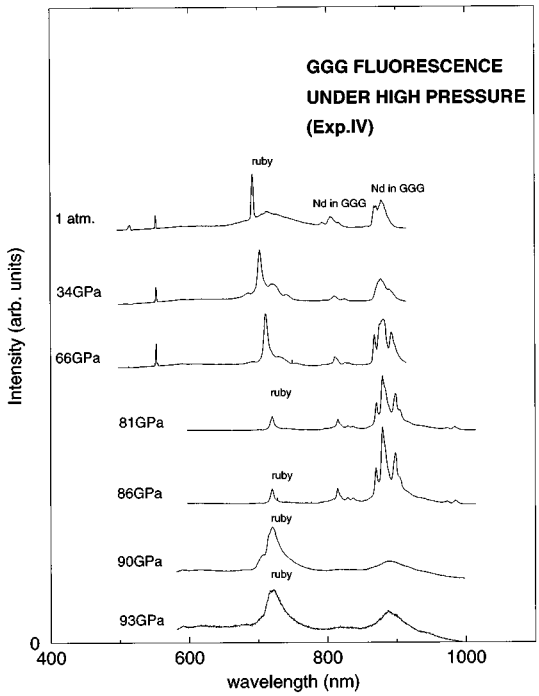


FIG. 8. Pressure dependence of the emission in $Nd^{3+}$, $Cr^{3+}$:GGG at room temperature, excited by argon 514.5 nm laser, ruby is the pressure sensor (Exp. IV). The spectrum covers the broad spectral range of 570–990 nm.

experiment, we attribute the broadening to the change in site symmetry in GGG.

The highest pressure we reached for Exp. V is only $86\pm2$ GPa and at that pressure the sample still has some strong and resolvable emission bands such as the $R_2$ line. The nature of the quenched samples of Exp. V was different from that of Exp. IV: the quenched sample in Exp. IV has broad emission bands, while in Exp. V, the spectrum of the quenched sample is nearly identical to the original one.

#### *2. X-ray diffraction*

In the x-ray-diffraction experiment, as pressure increased, the sample's cubic lattice was changed from $12.52\pm0.03$ Å at ambient pressure to $11.48\pm0.04$ Å at a pressure of $74\pm3$ GPa. As pressure increased from $74\pm3$ to $84\pm4$ GPa, the sample's diffraction significantly broadened, which indicates that the sample became amorphous. The quenched sample retained its amorphous state (Fig. 9). The measured compression for the cubic phase of GGG at $74\pm3$ GPa is 22.9 $\pm0.5\%$.

### C. YAG

#### *1. Photoluminescence*

The photoluminescence experiment (Exp. VI) on $Nd^{3+}$:YAG was conducted up to $72\pm2$ GPa, as shown in Fig. 10, employing 150 grooves/mm grating. Using higher resolution 1200 grooves/mm grating, the spectra in Fig. 11 show the pressure effect on the transition $^4F_{3/2}\rightarrow{}^4I_{9/2}$ of $Nd^{3+}$ in YAG. It is clear that from Fig. 11, the $R_1$ and $R_2$ lines broaden slightly as pressure increases while the other bands broaden wider, especially after $25.0\pm0.5$ GPa. At $72\pm2$ GPa, the $R_1$ and $R_2$ lines become the most intense bands in this region. The sample returned back to its original state after totally releasing the pressure.

#### *2. X-ray diffraction*

An x-ray-diffraction experiment was performed up to $101\pm4$ GPa, and the sample retained cubic structure throughout the experiment. The YAG lattice changes from

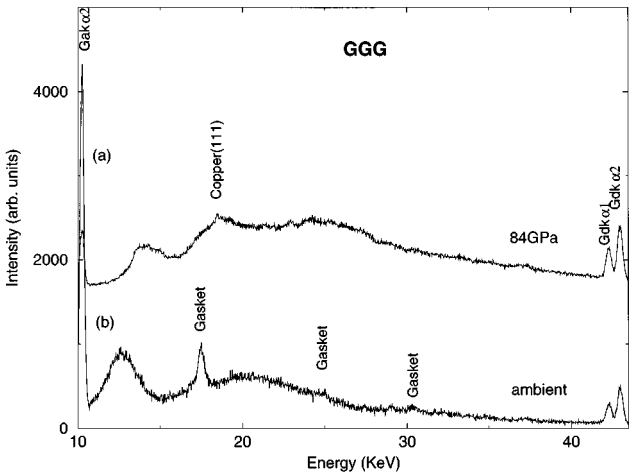


FIG. 9. Energy-dispersive x-ray-diffraction spectra obtained at the $B1$ station, CHESS of the GSGG sample mixed with copper pressure standard. $Ed=35.137$ KeV Å. (a) spectrum at $84\pm4$ GPa in the amorphous phase showing only weak marker (copper) peak (b) ambient pressure spectrum after decompression from $84\pm4$ GPa. The sample is still in the amorphous state.

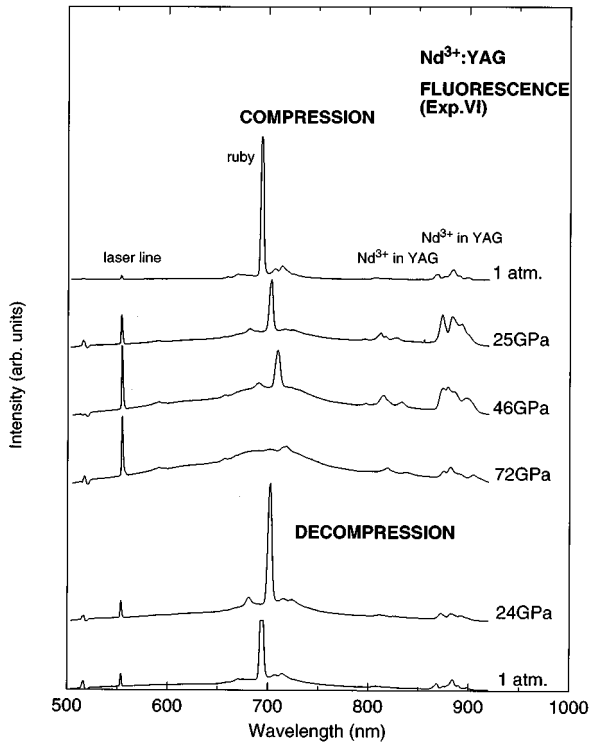


FIG. 10. Pressure dependence of the emission in ($Nd^{3+}$:YAG at room temperature, excited by argon 514.5 nm, ruby is the pressure sensor). The changes in spectrum in this sample are reversible on decompression.

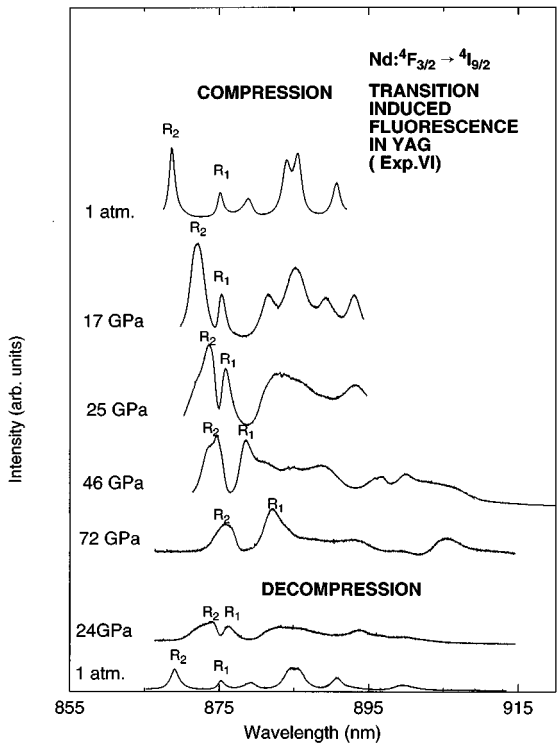


FIG. 11. High-resolution scans of the $Nd^{3+}$ $^4F_{3/2} \rightarrow {}^4I_{9/2}$ photoluminescence spectra of $Nd^{3+}$:YAG at various pressures, the labels $R_2$ and $R_1$ are defined in Fig. 2(b).

$12.00 \pm 0.05$ Å at ambient pressure to $11.00 \pm 0.03$ Å at $101 \pm 4$ GPa, with the compression of $23.0 \pm 0.5\%$. The sample recovers its initial cubic structure after quenched from the highest pressure.

## V. DISCUSSION

### A. Amorphization

According to the three-level diagram for $c \rightarrow a$ transition, if there is no intervention of metastable phases, the system would go to the lowest free-energy state, which is the crystalline phase. It has been proposed before that this stable crystalline phase is a phase mixture which resulted from the following decomposition path of $A_3B_2C_3O_{12}$ (Ref. 16):

$$A_3B_2C_3O_{12} \rightarrow 3ACO_3 + B_2O_3 \text{ (stable phase)},$$

where the $ACO_3$ is of perovskitelike structure and $B_2O_3$ of corundum structure. The laser heating experiment (Exp. X) on quenched amorphous GSGG shows that the stable phase for GSGG at ambient condition is single cubic phase. To document the existence of mixture as the stable phase, further laser heating experiments needed to be done at high pressure.

In photoluminescence experiments, after amorphization at $58 \pm 3$ GPa for GSGG and at $84 \pm 4$ GPa for GGG (documented by the x-ray-diffraction experiment), the samples' emission bands continue broadening and eventually become featureless, which means the materials lose their fine structures. If comparing our results on the three samples, GSGG, GGG, and YAG, and also combining the result that the emission bands for Sm:YAG abruptly broaden above 100 GPa, which was documented before,[1] we will find that in x-ray-diffraction experiments, the pressure at which the garnet amorphizes (which is $58 \pm 3$ GPa for GSGG and $84 \pm 4$ GPa for GGG) is related to the crystal-field strength of the garnet: *the lower the crystal-field strength, the lower the amorphization pressure.* In photoluminescence experiments, the process at which the emission bands spectra become featureless follows the same tendency: it is $77 \pm 2$ GPa for GSGG and $84 \pm 4$ GPa for GGG.

### B. Energy-level splittings

The pressure effect on the energy-level splittings is explained using crystal-field theory. We assume the crystal field at the $Nd^{3+}$ sites possesses three different symmetry components:

$$V = V_c + V_{nc} + V_n$$

where $V_c$ is the field component with cubic symmetry, $V_{nc}$ is field component with noncubic symmetry (including $D_2$ symmetry) and $V_n$ is component with no symmetry.

As we mentioned before, for state $^4F_{3/2}$ of $Nd^{3+}$ in garnet lattice, cubic symmetry gives no splitting, while symmetry lower than cubic will give the splitting as $R_1$ and $R_2$. Thus the component $V_{nc}$ as well as the component $V_n$ contribute to the splitting of $R_1$ and $R_2$, while the component $V_c$ tends to merge them together. Figure 12 compares the pressure effects on these two energy levels ($R_1$ and $R_2$) of $Nd^{3+}$ in GSGG, GGG, and YAG, with the data taken from Exp. I, Exp. IV, and Exp. VI, respectively. From this figure, we

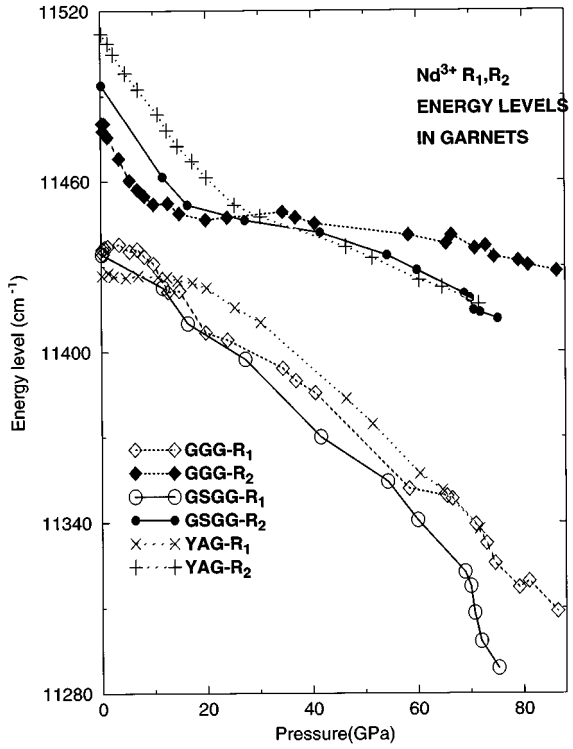


FIG. 12. The $R$-line splitting of $Nd^{3+}$ ($R_2$ and $R_1$) in GSGG, GGG, and YAG with increasing pressure. In all three garnets the splitting first decreases and then increases with increasing pressure.

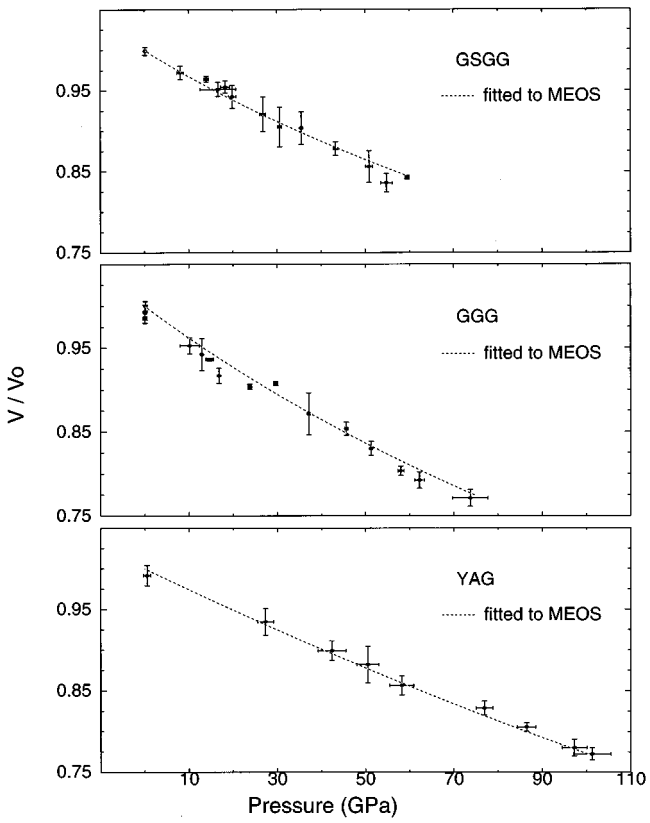


FIG. 13. The measured pressure-volume ($P$-$V$) curve for GSGG, GGG, and YAG at ambient temperature obtained from x-ray-diffraction data. The dashed curves are the fit to the modified equation of state discussed in the text [Eq. (1)].

notice that in all the three garnets, the two $R$ lines of $Nd^{3+}$ first come closer as pressure increases: the minimum splitting is at around 10 GPa in GSGG, 15 GPa in GGG and about 25 GPa in YAG. This indicates that there is a tendency toward a cubic site symmetry for $Nd^{3+}$ in the garnet lattice at low pressure around 15 GPa. After that, the two $R$ lines split further apart with increasing pressure, implying noncubic symmetry $V_{nc}$ and no symmetry $V_n$ components dominate. Since GSGG, GGG eventually lose their fine structures at $77\pm2$ and $86\pm2$ GPa, respectively, we deduce that near those pressures, no symmetry $V_n$ component contributes strongly to the splitting. The minimum splitting of $R_1$, $R_2$ lines is less in GGG than that in GSGG, which implies that the $Nd^{3+}$ in a GGG lattice experiences a stronger cubic symmetry component.

### C. Garnet lattice change

Figure 13 compares the $P$-$V$ properties of these three garnets: GSGG, GGG, and YAG obtained from synchrotron x-ray-diffraction experiments. The calculation of pressure error is explained previously in Sec. II E of this paper. The error in the measured compression ($V/V_0$) is estimated from the maximum fitting error in the diffraction peak location. The scatter in the experimental data in Fig. 13 is due largely to pressure averaging over the 30 $\mu$m x-ray beam size, which is not included in the current error calculation. It is clear from Fig. 13 that all the three oxide garnets show similar compression at high pressure within experimental errors. Equations of state for the three oxide garnets were fitted to Eq. (1). The fitted parameters ($B_0$,$B_0'$) are (294.0 GPa, 2.15), (253.3 GPa, 1.08), and (381.2 GPa, 0.05) for GSGG, GGG, and YAG, respectively.

### D. Decompression

In all the optical and x-ray experiments, we investigated the changes in the spectra during compression as well as after total decompression. We found that the nature of the quenched sample depends upon the maximum pressure reached. For optical experiments on GSGG, in Exp. I and Exp. II, where the sample's emission bands become featureless broad at the highest pressure, the sample is irreversible with pressure. In Exp. III with the highest pressure of 51.0 $\pm0.5$ GPa, at which the sample still has some sharp emission bands, the quenched sample has the same cubic phase as the original one. The same tendency occurs in GGG, i.e., the sample cannot go back to its original cubic phase if it is quenched from the highest pressure with all the emission bands being featureless. The optical experiment on YAG reaches $77\pm2$ GPa as the highest pressure and sample only has gradual broadening, the quenched sample returns back to its original crystalline phase. In x-ray experiment on GSGG and GGG, where *the samples undergo amorphization, they retain the amorphous state upon decompression*. The x-ray study on YAG has not shown amorphization and the sample is reversible with pressure.

### E. Application as pressure sensor

The application of any optical pressure sensor is generally limited to certain pressure and temperature region. Ruby's $R$ line is a well established pressure sensor and is used widely and well calibrated. All the three garnets we investigated show to be promising pressure sensor in the near-infrared region around 900 nm due to the $Nd^{3+}$ $^4F_{3/2} \rightarrow {}^4I_{9/2}$ emission bands. Among these bands, $R_2$ emission line remains sharp and intense at high pressure in all three garnets and seems to be the best line for calibration. However, since the garnets eventually lose their fine structures, all the emission bands including $R_2$ line, become very broad and featureless after certain high pressure and are not suitable for calibration. Because this occurs at $76\pm1$ GPa in GSGG and $88\pm2$ GPa in GGG, while YAG has stable cubic phase up to $101\pm4$ GPa, YAG is a better sensor than the other two. Also the singly doped YAG ($Nd^{3+}$:YAG) has advantage over codoped samples ($Nd^{3+}$,$Cr^{3+}$:GSGG and $Nd^{3+}$,$Cr^{3+}$:GGG) that the singly doped YAG has no overlapping emission in the $R$ region of the ruby.

## VI. SUMMARY AND CONCLUSIONS

We summarize below our high-pressure and high-temperature investigations on oxide garnets:

(1) *X-ray diffraction*: In energy-dispersive x-ray-diffraction studies, using copper as pressure calibrant, amorphization is observed at $58\pm3$ GPa in GSGG and at $84\pm4$ GPa in GGG. YAG is found to retain its crystalline cubic phase up to $101\pm4$ GPa.

(2) *Photoluminescence*: In photoluminescence measurements, we noticed at pressures beyond amorphization, garnets show featureless emission bands, which is due to the loss of fine structure. This occurs at $76\pm1$ GPa in GSGG and $88\pm2$ GPa in GGG.

(3) *Laser heating*: The amorphous GSGG sample quenched from high pressure is subjected to laser heating by the Nd:YAG laser. Heating above $3100\pm100$ K resulted in the crystallization to the cubic garnet phase. The decomposition of the garnet into perovskitelike and corundum structures is not observed in laser heating carried out at ambient pressure.

(4) *$P$-$V$ property*: All three oxide garnets show similar $P$-$V$ relation at ambient temperature. The compression (volume change) of about 17% is achieved by 55 GPa in all the oxide garnets we investigated.

## ACKNOWLEDGMENTS

This research is supported by National Science Foundation (NSF) Grant No. DMR-9403832. We sincerely appreciate the assistance of Professor Tasoltan Basiev and Professor Vyacheslav Osiko from the General Physics Institute of Russian Academy of Sciences, who generously provided us the sample, and Dr. J. Z. Hu of beam line X-17 C at NSLS. We also acknowledge experimental assistance of Jun Liu and beneficial theoretical discussion with Dr. Alex Dergachev, both from the University of Alabama in Birmingham (UAB), Physics Department. Research carried out (in part) at the NSLS Brookhaven National Laboratory, and Cornell High Energy Synchrotron Source (CHESS).

[1] J. Liu and Y. K. Vohra, Appl. Phys. Lett. **64** (25), 3386 (1994).

[2] U. Hömmerich and K. L. Bray, Phys. Rev. B **51**, 8595 (1995); **51**, 12 133 (1995).

[3] H. Hua, J. Liu, and Y. K. Vohra, J. Phys. C **8**, L 139 (1996).

[4] J. B. Gruber, M. E. Hills, C. A. Morrision, G. A. Turner, and M. R. Kokta, Phys. Rev. B **37**, 8564 (1988).

[5] P. R. Wamsley and K. L. Bray, J. Lumin. **59**, 11 (1994).

[6] T. Yagi and J. Susaki, *High-Pressure Research: Application to Earth and Planetary Sciences*, edited by Y. Syono and M. H. Manghnani (Terra Scientific Publishing Company, Tokyo, 1992), pp. 51–54.

[7] O. Mishima, L. D. Calvert, and E. Whalley, Nature (London) **310**, 393 (1984).

[8] S. K. Sikka, in the *Proceedings XIII AIRAPT Conference, Bangalore, India*, edited by A. K. Singh (Oxford and IBH, New Delhi, 1992), p. 254.

[9] G. Huber, K. Syassen, and W. B. Holzapfel, Phys. Rev. B **15**, 5123 (1977).

[10] M. Yamaga, B. Henderson, and K. P. O'Donnel, Phys. Rev. B **46**, 3273 (1992).

[11] H. K. Mao, P. M. Bell, J. W. Shaner, and D. J. Steinberg, J. Appl. Phys. **49**, 3276 (1978).

[12] G. Gu and Y. K. Vohra, Phys. Rev. B **47**, 11 559 (1993).

[13] R. G. McQueen, S. P. Marsh, J. W. Taylor, J. M. Fritz, and W. J. Carter, in *High Velocity Impact Phenomenon*, edited by R. Kinslow (Academic, New York, 1970), Chap. VII.

[14] Y. K. Vohra and S. S. Vagarali, Appl. Phys. Lett. **61**, 2680 (1992).

[15] D. L. Heinz, and R. Jeanloz, in *High-Pressure Research in Mineral Physics*, edited by M. H. Manghnani and Y. Syono (American Geophysical Union, Washington, D. C., 1987), pp. 113–127.

[16] M. Marezio, J. P. Remeika, and A. Jayaraman, J. Chem. Phys. **45**, 1821 (1966).